Available online at www.sciencedirect.com
SCIENCE DIRECT®
Journal of Power Sources 135 (2004) 249–254
JOURNAL OF POWER SOURCES
www.elsevier.com/locate/jpowsour

The usefulness of a $LiMn_2O_4$ composite as an active cathode material in lithium batteries

C. Polo Fonseca, S. Neves*

Laboratório de Caracterização e Aplicação de Materiais (LCAM), Universidade São Francisco, Campus Itatiba, São Paulo 13251-900, SP, Brazil

Received 9 March 2004; accepted 29 March 2004

Available online 10 June 2004

Abstract

The synthesis and electrochemical properties of a lithium manganese spinel, a $LiMn_2O_4$ film and a $LiMn_2O_4$/polyaniline (PAni)/PVDF composite film were investigated. The materials were characterized using X-ray diffraction, differential thermal analysis, scanning electron microscopy and BET surface area analysis. The intercalation/deintercalation lithium was investigated using electrochemical impedance spectroscopy, cyclic voltammetry and charge/discharge cycles. The use of PAni as an electronic conductor and electroactive material optimized the process of lithium intercalation/deintercalation in this film. The stabilized lithium extraction capacity of the $LiMn_2O_4$/PAni/PVDF composite was significantly higher than for the $LiMn_2O_4$ film (138 and 52 mA h g^{-1}, respectively).

Keywords: $LiMn_2O_4$; Polyaniline; Composite; Lithium battery

1. Introduction

Batteries are widely used in portable instruments, remote controls, solar power packs, pacemakers and toys, and there is an increasing demand for rechargeable batteries with a high specific energy and power. In recent decades, many new materials and methods of fabrication have been developed for the cathode thin films used in microbatteries [1]. Lithium metal oxides with a layered structure are the most promising materials [2]. $LiCoO_2$ is currently used as a cathode material in commercial, rechargeable lithium batteries because of its high specific capacity, high operating cell voltage and excellent re-chargeability. However, the use of $LiCoO_2$ is compromised by the cost of the batteries since only half of the lithium can be retrieved from $LiCoO_2$ in a form suitable for reuse [3,4]. The toxicity, the high cost of cobalt oxide, and the methods of synthesis (usually involving prolonged heating of lithium and cobalt oxides, or their carbonates or nitrates, at 800–900 °C) also contribute to the overall high cost of these batteries. $LiNiO_2$ is another attractive candidate for cathode material because of the natural abundance of nickel and its environmentally safeness. However, $LiNiO_2$ is difficult to synthesize with consistent quality because of its tendency to undergo non-stoichiometric reactions and shows poor recycling performance because of its structural instability. Nickel also poses greater safety problems [5–8]. For these reasons, batteries with $LiNiO_2$ as the cathode material are not yet available commercially.

Lithium manganese oxide ($LiMn_2O_4$) has received much attention as a cathode material because of the high voltage required for lithium insertion as well as its lower price, availability and better compliance with environmental regulations compared to $LiCoO_2$ and $LiNiO_2$ [9–13]. However, $LiMn_2O_4$ often shows a low storage capability, even at higher temperatures, and a significant loss of capacity during extended cycling in the 3–4 V region. A shift from a tetragonal to a cubic structure occurs when the average manganese valency reaches about 3.5. The critical concentration of Mn^{3+} leads to the Jahn–Teller distortion responsible for the change that causes the structural instability of $Li_xMn_2O_4$ compounds during cycling [14–16]. The loss of this capacity during electrochemical cycling has been the major factor limiting the commercialization of Li-ion cells with $Li_xMn_2O_4$ as a positive electrode.

Following the discovery by Shirakawa et al. [17] that virgin polyacetylene can be reversibly oxidized and reduced, and thus be switched reversibly from an insulating to a

* Corresponding author. Tel.: +55-11-4534-8071; fax: +55-11-4524-1933.
E-mail address: silmara.neves@saofrancisco.edu.br (S. Neves).

0378-7753/$ – see front matter © 2004 Elsevier B.V. All rights reserved.
doi:10.1016/j.jpowsour.2004.03.057

semiconducting or conducting state, numerous attempts have been made to use the redox reactions of conducting polymers for charge storage [18]. Conducting polymers, such as polyaniline (PAni), conduct electricity principally by the movement of charge carriers known as polarons and bipolarons generated when the polymer is slightly oxidized [19]. Thus, the combination of these two types of materials generates a class of mixed conduction composites with unique properties and relatively simple synthetic procedures. A transition metal oxide-conducting polymer composite shows increased capacity because of the doping/undoping of ions in the conducting polymer. The use of a chemically prepared $LiMn_2O_4$–polypyrol composite cathode in liquid electrolytes has been reported [20]. Recently, Kim et al. [21] investigated the charge/discharge cycling characteristics of $LiMnO_2$–PAni–DMcT composites with a polymer electrolyte and found a good capacity (126 mA h g^{-1}) and efficiency with cycling (98% after the seventh cycle). In both cases, carbon was partially substituted by the conductor polymer.

In this paper, we examined the usefulness a $LiMn_2O_4$/PAni/PVDF composite as a new cathode material in lithium batteries. Only polyaniline was used as an electronic conductor. The synthesis and physical and electrochemical properties of $LiMn_2O_4$ and composite films are reported.

2. Experimental

2.1. Synthesis of $LiMn_2O_4$

$LiMn_2O_4$ was synthesized via a precipitation reaction of aqueous solutions of $Mn(NO_3)_2$ and LiOH with 1.0 mol L^{-1} NH_4OH (all from Aldrich). The molar ratio of Li and Mn, the two reactants, was 1:1. The resulting powder was dried and heated at 250 °C for 4 h.

2.2. Synthesis of PAni powder

The polyaniline powder was prepared chemically as described elsewhere [22].

2.3. Preparation of films

Two types of films were prepared. A cathode electrode was obtained by mixing $LiMn_2O_4$ powder (95 wt.%) with poly(vinylidene fluoride) (PVDF; 5 wt.%; Fluka, MW = 10^5 g mol^{-1}) in *N*,*N*-dimethyl acetamide. The composite electrode were prepared by mixing $LiMn_2O_4$ powder, polyaniline (15 wt.%) and poly(vinylidene fluoride) (5 wt.%) in *N*,*N*-dimethyl acetamide. The films were obtained by spin-coating (5000 rpm, 5 s) each mixture on glass plates coated with a thin film indium-tin oxide (ITO). Prior to use, the electrodes were dried at 120 °C in a vacuum furnace for 1 h.

2.4. Physical characterization

The oxide powder was characterized by X-ray diffraction (XRD) using Ni-filtered Cu Kα radiation (0.8 kW) in the step scanning mode, with steps of 0.05°. The counting time was 10 s for the entire spectrum, $15° \leq 2\theta \leq 65°$. The specific surface area of the oxide was measured by the Brunauer–Emmett–Teller (BET) method using N_2 gas.

Differential thermal analysis (DTA) was done with the oxide, polyaniline and the composite at a heating rate of 5 °C min^{-1} up to 800 °C in N_2, using a NETZSCH DTA 404 EP analyzer. The morphology of all samples was examined by scanning electron microscopy (SEM).

2.5. Electrochemical measurements

Electrochemical tests were done in liquid electrolyte at room temperature using 1 mol L^{-1} $LiClO_4$ in 1:1 mixtures of ethylene carbonate (EC) and propylene carbonate (PC). The electrodes were cycled in cells with 200 mm thick lithium foil as the negative electrode. The electrochemical cells were cycled in the range of 3.0–4.3 V, with $v = 5$ mV s^{-1} and a charge/discharge current density of 10 μA cm^{-2}. An ac amplitude of 10 mV was used for electrochemical impedance spectroscopy.

To assess the conductivity, the materials were compressed by blocking electrodes. The frequency used ranged was from 10^5 to 1 Hz. The intercalation/deintercalation of lithium was examined using a liquid cell configuration and a frequency ranging from 10^5 to 10^{-2} Hz. All electrochemical experiments were done in an argon-filled dry box using an AUTOLAB–PGSTAT30 FRA.

3. Results and discussion

3.1. Characterization of the materials

There was considerable variation in the structure of lithium manganese oxide, indicating the thermodynamic stability of the crystalline structure. However, when the phase formation occur under elevated temperature, may it is not be stable at room temperature.

The DTA profile of the powder oxide is shown in Fig. 1. A broad exothermic peak at about 105 °C was associated with water evaporation and another at 220 °C was probably related to the crystallization peak of $LiMn_2O_4$. The endothermic peak of the profile probably reflected the presence of residual reagents (LiOH) [23]. The crystalline structure of the material was verified by XRD analysis (Fig. 2).

The XRD data also revealed the formation of $LiMn_2O_4$. All of the diffraction peaks for this material were assigned to the diffraction indices of the $LiMn_2O_4$ single-phase spinel [24–26] at 250 and at 400 °C, in agreement with the DTA results. The advantages of the precipitation technique used to produce $LiMn_2O_4$ include a high specific surface area

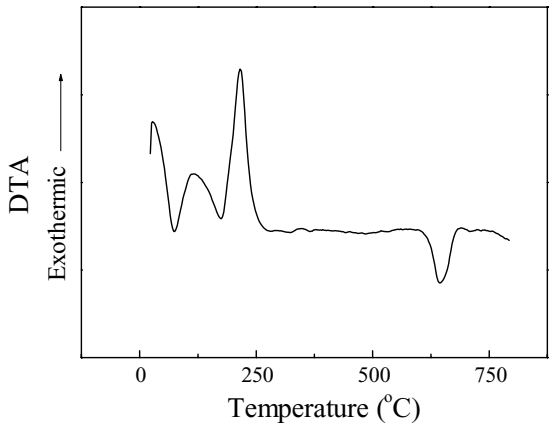

Fig. 1. Differential thermal analysis of the lithium manganese oxide at a heating rate of 5 °C min^{-1}.

and the ease with which the ratio of lithium to manganese can be controlled at low temperature. The particle size of the cathode material is a very important factor in the lithium intercalation/deintercalation process, with smaller particles improving the cell re-chargeability and the specific capacity. After this analysis, the powder was dried under vacuum in a furnace at 250 °C for 4 h to guarantee the formation of $LiMn_2O_4$.

The morphologies of the lithium manganese oxide, polyaniline and composite powders were examined by SEM (Fig. 3). A homogeneous distribution of $LiMn_2O_4$ particles with a diameter of about 80 nm (Fig. 3a), and larger agglomerates of polyaniline (Fig. 3b) were observed. The composite consisted of small oxide particles which were slightly fused with polyaniline to form larger agglomerates of 5–15 μm.

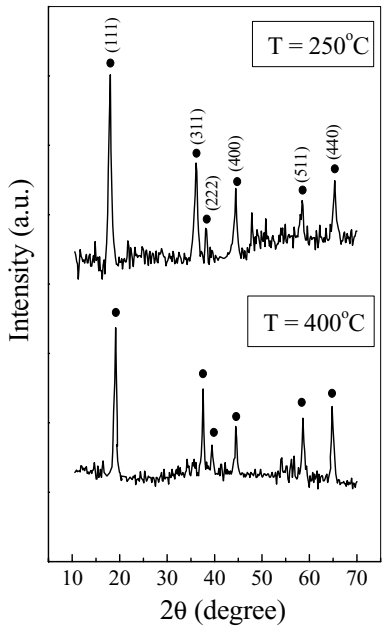

Fig. 2. XRD data of the $LiMn_2O_4$ counting time = 10 s in the range $15^\circ \leq 2\theta \leq 65^\circ$.

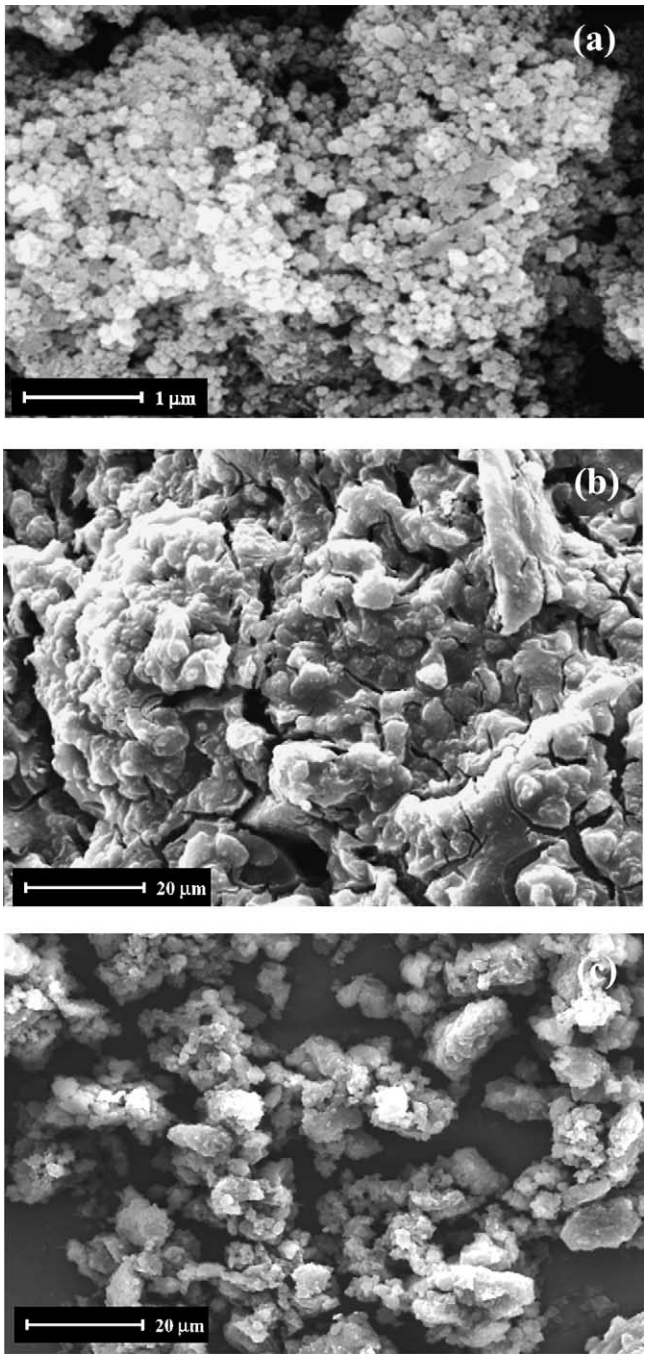

Fig. 3. Scanning electron micrographs of a (a) $LiMn_2O_4$, (b) PAni and (c) $LiMn_2O_4$/PAni powders.

The specific surface area of $LiMn_2O_4$ was 79.54 ± 4.95 m^2 g^{-1}, comparable to that obtained by mechanochemical synthesis [23]. For polyaniline, the specific surface area was 7.64 ± 0.01 m^2 g^{-1}.

3.2. Electrochemical behavior

Impedance analysis was used to obtain information about the conductivity and the process of lithium intercalation/deintercalation. In the first case PAni and $LiMn_2O_4$

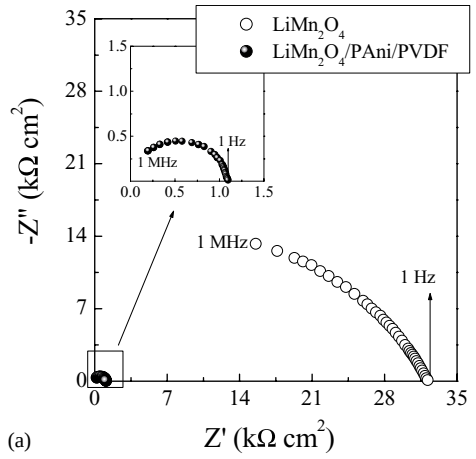

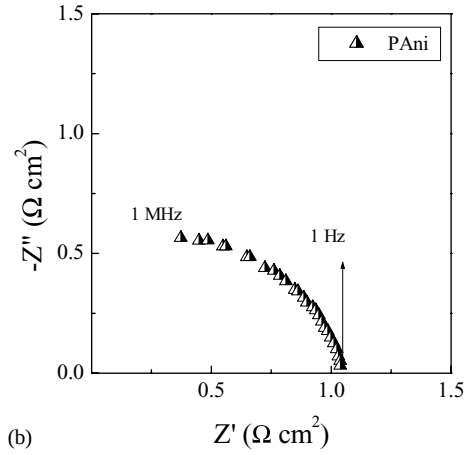

Fig. 4. Nyquist diagram of $LiMn_2O_4$ and a $LiMn_2O_4$/PAni/PVDF composite (a) and PAni (b) using a blocking electrode. Perturbation amplitude is 0.01 V and the frequency range from 10^5 to 1 Hz.

powders and composite film were analyzed (Fig. 4). Only one semicircle was observed in the open-circuit potential (OCP) state for all samples. No other semicircle and no increase in the Z'' value was observed at lower frequencies. Thus, conductivity was considered to have an electronic character. The bulk resistance was obtained from the impedance spectra at the point where the arc intercepts the real part in the low frequency region. The conductivity was calculated using the equation

$$\sigma = \frac{\ell\,(\mathrm{cm})}{Z\,(\Omega)\cdot A\,(\mathrm{cm}^2)} \quad (1)$$

where ℓ is the material thickness (a spacer thickness of 40 μm was used to keep the thickness constant), Z is the impedance estimated from the Nyquist plot and A is the stainless steel electrode area (1 cm^2) covered by the material.

Inorganic oxide materials generally have a low electronic conductivity and are mixed with active carbon to improve this property. In agreement with this, the conductivity of $LiMn_2O_4$ was relatively low (3.1×10^{-6} S cm^{-1}). In the composite cathode, PAni substituted for carbon and yielded an electroactive material with a potential similar to that of $LiMn_2O_4$ [27]. The conductivity of the PAni powder was 0.1 S cm^{-1}.

Comparison of the behavior of the three samples showed that the addition of PAni increased the conductivity of the composite material by about 100 times, as indicated by the decrease in composite impedance (Fig. 4a, inset). The $LiMn_2O_4$/PAni composite had a conductivity of about 1×10^{-4} S cm^{-1}.

The electrochemical intercalation/deintercalation of Li in the $LiMn_2O_4$ film and $LiMn_2O_4$/PAni/PVDF composite film was analyzed by cyclic voltammetry (Fig. 5). According to Xia and Yoshio [28], the extraction of Li from both systems of $LiMn_2O_4$ is accompanied by the oxidation of Mn^{3+} to Mn^{4+} and by a decrease in volume of approximately 7.5% between the starting material and the fully extracted spinel. When the intercalation/deintercalation cycles occur repeatedly, the intercalation sites of the lithium ion can be collapsed, resulting in a decrease in the charge capacity of the material.

In Fig. 5 we can see two intercalation/deintercalation process illustrated by two pairs of redox peaks at high potential range in the cyclic voltammogram related to the deintercalation of Li at 4.0 and 4.2 V versus Li and the inter-

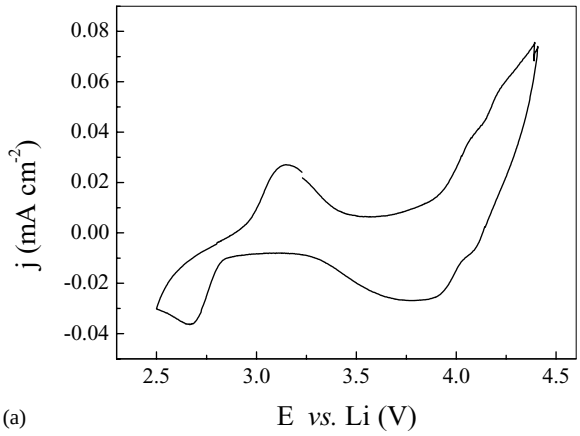

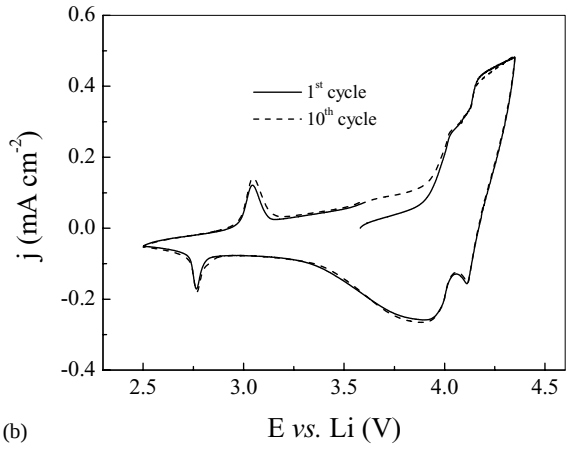

Fig. 5. Steady-state cyclic voltammogram of a $LiMn_2O_4$ film (a) and a $LiMn_2O_4$/PAni/PVDF film (b) in PC/EC/1 mol L^{-1} $LiClO_4$, at 5 mV s^{-1}.

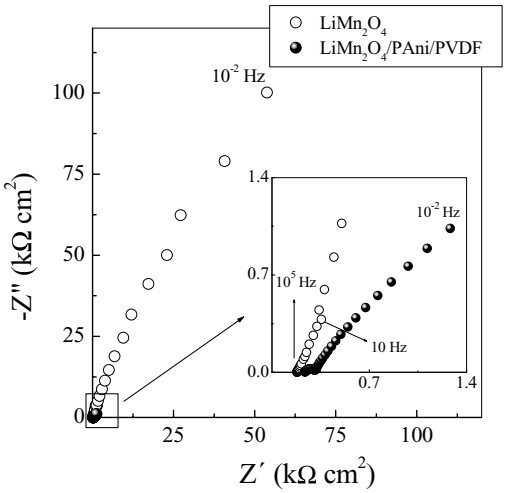

Fig. 6. Nyquist diagram of pure $LiMn_2O_4$ and a $LiMn_2O_4$/PAni/PVDF composite in PC/EC/1 mol L^{-1} $LiClO_4$ at 4.0 V. Perturbation amplitude is 0.01 V and the frequency range from 10^5 to 10^{-2} Hz.

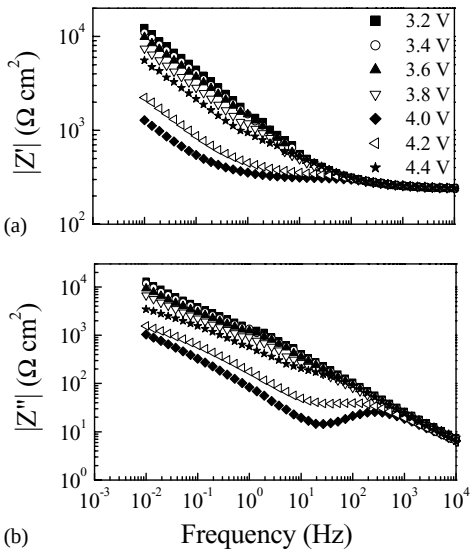

Fig. 7. Frequency dependence of impedance, real part (a) and imaginary part (b), obtained at different potentials in PC/EC/1 mol L^{-1} $LiClO_4$. Perturbation amplitude is 0.01 V and the frequency range from 10^5 to 10^{-2} Hz.

calation of Li at 3.9 and 4.1 V, in agreement with previous reports [29,30]. That lithium can be extracted in two steps can be explained by its spinel structure [31]. This process was intensified and defined better in the composite film than pure $LiMn_2O_4$ film (Fig. 5b). One possible interpretation for this intensification of the redox peaks of $LiMn_2O_4$ is the effective participation of PAni as an electronic conductor and electroactive material, thereby optimizing the process of lithium intercalation/deintercalation. The composite film also showed a very high electrochemical stability, as seen by comparison of the 1st and 10th voltammetric cycles. The 3.1/2.8 V peak seen in both films was related to the coexistence of cubic and tetragonal phases of manganese oxide [32].

Impedance analysis of the $LiMn_2O_4$ and $LiMn_2O_4$/PAni/PVDF composite films at 4.0 V versus Li was used to compare the impedance under charge conditions (Fig. 6). In the oxide impedance spectrum, only the imaginary part increased with decreasing frequency, as a result of the capacitive response. In contrast, in the composite spectrum, a semicircular arc appeared in the high frequency range related to charge transfer reactions at the interface of the electrolyte/composite electrode. The inclined line in the low frequency range was attributed to 'Warburg impedance' associated with lithium diffusion through the composite electrode [33]. The impedance of the pure system was higher than that of the composite film (100.2 and 1.3 kΩ cm^2, respectively). This difference was attributed to the presence of PAni in this composite, which increased the electronic conductivity of the film by acting as electroactive material.

The variation in impedance as a function of the potential or lithium deintercalation process was assessed only for the composite film. The EIS measurements were done at fixed potentials from 3.2 to 4.4 V in 200 mV intervals. At each potential, the dc current response was monitored to ensure that the $LiMn_2O_4$/PAni/PVDF electrode reached equilibrium at a given potential prior to the EIS measurements. To observe the impedance behavior better, we plotted the EIS data in a Bode-type plot (Fig. 7a and b). The real impedance values determined in the plateau (about 243 Ω cm^2) at high frequency were related to the organic electrolyte resistance. As the applied potential increased, the impedance of the system became smaller, until a minimum was reached at 4.0 V, after which the impedance gradually increased again (Fig. 8). This inversion may be related to a non-homogeneous extraction of lithium (compare the drop in impedance between 3.8 and 4.0 V) and the over-oxidation of polyaniline. The first lithium deintercalation process observed in cyclic voltammetry (Fig. 5) occurred exactly at this potential, the second redox peak at approximately 4.2 and 4.4 V has a high impedance value indicating a difficult in the lithium deintercalation, beside to be the potential where PAni showed low conductivity (pernigraniline state).

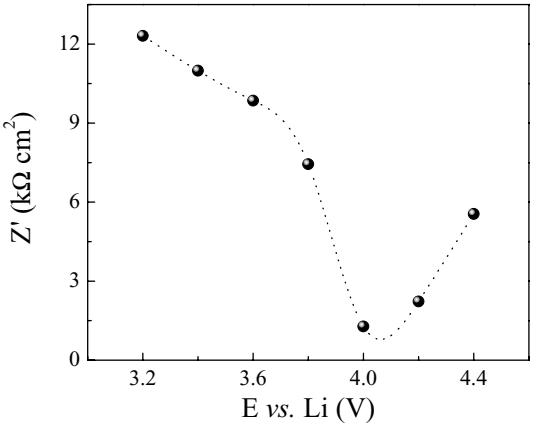

Fig. 8. Impedance variation as a function of the potential applied to the $LiMn_2O_4$ composite film in PC/EC/1 mol L^{-1} $LiClO_4$.

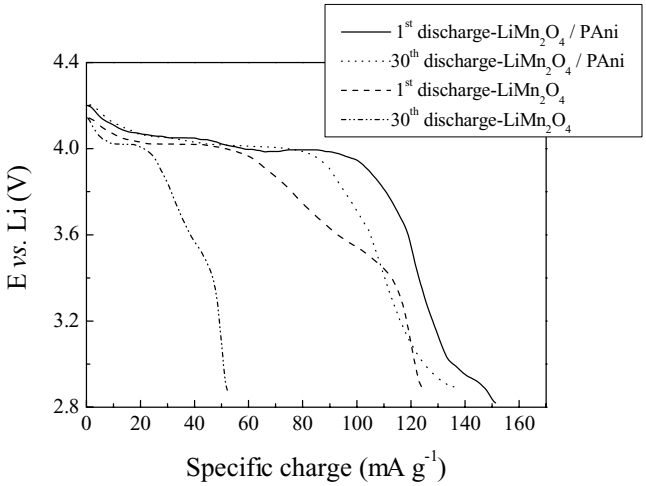

Fig. 9. Specific discharge capacity of $LiMn_2O_4$ and $LiMn_2O_4$/PAni/PVDF films in the 1st and 30th discharge cycles: $j = 10\,\mu A\,cm^{-2}$.

A similar behavior was seen in the Bode plots of the imaginary part of the EIS (Fig. 7b), where the peak values corresponded to the radius of the semicircular arcs observed at 4.0 V and related to the charge transfer process in the composite electrode/electrolyte interface.

To investigate the performance of the battery, we used $LiMn_2O_4$ and $LiMn_2O_4$/PAni/PVDF films as the cathode. The discharge curves for both films operating between 4.2 and 2.8 V are shown in Fig. 9. All films were tested at a constant current density ($10\,\mu A\,cm^{-2}$). As expected, the $LiMn_2O_4$/PAni/PVDF composite had a better discharge response than did the $LiMn_2O_4$ film. For the composite film, the discharge in the first cycle was $153\,mA\,h\,g^{-1}$ and reached a stable value of $138\,mA\,h\,g^{-1}$ after the 30th cycle. In contrast, the initial discharge capacity for the $LiMn_2O_4$ film was $121\,mA\,h\,g^{-1}$ and then stabilized at $52\,mA\,h\,g^{-1}$.

The difference observed in the discharge capacity of the two electrodes used here can be explained by the use of polyaniline combined with $LiMn_2O_4$, which increases the conducting path in addition to supporting the structural reversibility.

4. Conclusion

$LiMn_2O_4$ and $LiMn_2O_4$/PAni/PVDF films were produced by a precipitation method using spin-coating and annealing at low temperature. The $LiMn_2O_4$ powder showed a high specific surface and the composite film was homogeneous. The electrochemical properties of the two films were compared and the composite showed the best performance because of the presence of PAni that acted as an electronic conductor and improved the conductivity of $LiMn_2O_4$. PAni also served as an electroactive material that increased the charge/discharge capacity of the composite film. The presence of PAni increased the stabilized discharge capacity of the composite film by more than two-fold relative to the pure $LiMn_2O_4$ film. Overall, the composite showed good electrochemical performance as a cathode for use in lithium batteries.

Acknowledgements

This work was supported by FAPESP (grant number 98/14756-8).

References

[1] S.D. Jones, J.R. Akridge, Solid State Ionics 69 (1994) 357.
[2] R.M. Dell, Solid State Ionics 134 (2000) 139.
[3] G.G. Amatucci, J.M. Tarascon, L.C. Klein, J. Electrochem. Soc. 143 (1996) 1114.
[4] N. Imanishi, M. Fujii, A. Hirano, Y. Takeda, M. Inaba, Z. Ogumi, Solid State Ionics 140 (2000) 45.
[5] S.P. Sheu, I.C. Shih, C.Y. Yao, J.M. Chen, W.M. Hurng, J. Power Sources 68 (1997) 558.
[6] R.V. Moshtev, P. Zlatilova, S. Vasilev, I. Bakalova, K. Tagawa, A. Sato, Prog. Batt. Batt. Mater. 16 (1997) 168.
[7] H. Arai, S. Okada, Y. Sakurai, J.-I. Yamaki, Solid State Ionics 95 (1997) 275.
[8] R.V. Moshtev, P. Zlatilova, V. Manev, A. Sato, J. Power Sources 54 (1995) 329.
[9] Y. Xia, Y. Zhou, M. Yoshio, J. Electrochem. Soc. 144 (1997) 2593.
[10] K. Oikawa, T. Kamiyama, F. Izumi, B. Chakoumakos, H. Ikuta, M. Wakihara, J. Li, Y. Matsui, Solid State Ionics 109 (1998) 35.
[11] Y.-S. Han, H.-G. Kim, J. Power Sources 88 (2000) 161.
[12] Y.W. Tsai, R. Santhanam, B.J. Hwang, S.K. Hu, H.S. Sheu, J. Power Sources 119–121 (2003) 701.
[13] W.T. Jeong, J.H. Joo, K.S. Lee, J. Power Sources 119–121 (2003) 690.
[14] A. Yamada, M. Tanaka, Mater. Res. Bull. 30 (1995) 715.
[15] H. Yamaguchi, A. Yamada, H. Uwe, Phys. Rev. B 58 (1998) 8.
[16] Y.M. Hon, K.Z. Fung, M.H. Hon, J. Eur. Ceram. Soc. 21 (2001) 515.
[17] H. Shirakawa, E.J. Louis, A.G. MacDiarmid, C.K. Chiang, A.J. Heeger, J. Chem. Soc. Chem. Commun. (1977) 578.
[18] P. Novák, K. Müller, K.S.V. Santhanam, O. Haas, Chem. Rev. 97 (1997) 207.
[19] D.C. Trivedi, Handbook of Organic Conductive Molecules and Polymers, vol. 2, John Wiley & Sons, Chichester, 1997.
[20] A.H. Gemeay, H. Nishiyama, S. Kuwabata, H. Yoneyama, J. Electrochem. Soc. 142 (1995) 4190.
[21] J.-U. Kim, Y.-J. Jo, G.-C. Park, W.-J. Jeong, H.-B. Gu, J. Power Sources 119–121 (2003) 686.
[22] W.A. Gazotti, M.-A. De Paoli, Synth. Met. 80 (1996) 263.
[23] N.V. Kosova, N.F. Uvarov, E.T. Devyatkina, E.G. Avvakumov, Solid State Ionics 135 (2000) 107.
[24] S.R.S. Prabaharan, M.S. Michael, T.P. Kumar, A. Mani, K. Athinarayanasway, R. Gangadharan, J. Mater. Chem. 5 (1995) 1035.
[25] T. Tsumura, A. Shimizu, M. Inagaki, J. Mater. Chem. 3 (1993) 995.
[26] C.-H. Lu, S.K. Saha, Mater. Sci. Eng. B 79 (2001) 247.
[27] A. Malinauskas, Polymer 42 (2001) 3957.
[28] Y. Xia, M. Yoshio, J. Electrochem. Soc. 143 (1996) 825.
[29] J.M. Tarascon, W.R. Mckinnon, T.N. Bowmer, G. Amatucci, D. Guymond, J. Electrochem. Soc. 141 (1994) 1421.
[30] P. Barbox, J.M. Tarascon, F.K. Shokoohi, J. Solid State Chem. 94 (1991) 185.
[31] K. Huang, B. Peng, Z. Chen, P. Huang, Sol. Energy Mater. Sol. Cells 62 (2000) 177.
[32] K.H. Hwang, S.H. Lee, S.K. Joo, J. Power Sources 54 (1995) 224.
[33] Y.M. Choi, S.I. Pyun, Solid State Ionics 99 (1997) 173.